Supporting Information: Elucidating the Nuclear Quantum Dynamics of Intramolecular Double Hydrogen Transfer in Porphycene

Yair Litman,[†] Jeremy O. Richardson,[‡] Takashi Kumagai,[¶] and Mariana Rossi[*,†]

†*Theory Department, Fritz Haber Institute of the Max Planck Society, Faradayweg 4–6, 14195 Berlin, Germany*

‡*Laboratory of Physical Chemistry, ETH Zurich, 8093 Zurich, Switzerland*

¶*Physical Chemistry Department, Fritz Haber Institute of the Max Planck Society, Faradayweg 4–6, 14195 Berlin, Germany*

E-mail: rossi@fhi-berlin.mpg.de

Additional Information on Electronic Structure Calculations

Our reference calculations were computed with DLPNO-CCSD(T) method[1] on top of MP2[2] relaxed structures. These simulations were performed with the ORCA package.[3] We used resolution of the identity (RI) for the coulomb and the correlation exchange term were treated via seminumerical integration (COSX). The convergence criteria was set to "TIGHTSCF". We used the Dunning's correlation consistent (cc-) polarized (p) Valence (V) Double-Zeta (DZ), Triple-Zeta (TZ), Quadruple-Zeta (QZ) and 5-zeta (5Z) basis sets.[4] We used the interpolation scheme by Karton and Martin[5] for the mean field (or Hartree Fock) energy and the scheme by Truhlar[6] for the correlation energy at the MP2 level. Note that this is a

3 point interpolation.

Regarding DFT calculations, three exchange correlation (xc) functionals, namely PBE,[7] PBE0[8] and B3LYP,[9,10] and two types of dispersion interactions corrections (Tkatchenko-Scheffler (TS)[11] and many body dispersion (MBD)[12] were tested. All the density functional electronic structure calculations were performed using the all-electron FHI-aims program[13] with both *light* and *tight* settings. These default settings include both the size of the basis sets as well as other numerical parameters and are readily available with the program package.

In Table S1 and Table S2 we show the energy and relevant geometric parameters for all the stationary points obtained with the different xc functionals and CCSD(T). We present here only the results obtained with *light* settings. Their difference with respect to *tight* settings was, in all the cases, below 5 meV for energies differences and 0.01 for geometrical parameters. We note that for the three xc functionals tested, dispersion interactions play a minor role in the relative energies, in most cases representing differences below 5 meV. Zero point energy (ZPE) contributions were only computed for the functionals including the TS dispersion correction. All xc functionals predict a potential energy surface (PES) which is characterized by two pairs of degenerate local minima, 4 first order saddle point and 1 second order in agreement with the literature.[14,15] B3LYP+TS is the only functional where both barriers are still present after the ZPE corrections and, therefore, does not predict a 'trivial' delocalization of the hydrogen between the two trans states.

Table S1: Energy of the stationary points of the porphycene potential energy surface for different theory levels. Number in parenthesis are ZPE corrected. Trans, cis, SP1 and SP2 structures are defined in the Fig. 1 of the main text. The zero of energy is set at the trans geometry for each setting and the energies are expressed in meV.

	PBE	PBE+TS	PBE+MBD	PBE0	PBE0+TS
cis	73	72 (35)	70	90	89 (60)
SP1	110	106 (-14)	102	157	155 (29)
SP2	154	150 (-61)	142	233	228 (-1)
	PBE0+MBD	B3LYP+TS	MP2	CCSD(T)	
cis	86	93 (72)	104(51)	160	
SP1	150	189 (62)	144(2)	218	
SP2	216	290 (56)	194(-47)	322	

Table S2: Relevant geometric parameters of the stationary points of the porphycene PES. Distances are expressed in Ångstroms. Trans, cis, SP1 and SP2 structures as well as δ_1, δ_2, d_1, d_2, d_3 and d_4 are defined in the Fig. 1 of the main text.

	B3LYP			
	δ_1	δ_2	d_1,d_3	d_2,d_4
Trans	-0.55	-0.55	2.65	2.83
Cis	-0.55	0.55	2.61	2.88
SP1	-0.53	0.04	2.58	2.88
SP2	0.00	0.00	2.50	2.88
Exp.[16]	–	–	2.63	2.83
	MP2			
	δ_1	δ_2	d_1,d_3	d_2,d_4
Trans	-0.57	-0.57	2.62	2.82
Cis	-0.46	0.46	2.57	2.88
SP1	-0.45	0.08	2.50	2.88
SP2	0.00	0.00	2.49	2.87

In Table S3 we show the average absolute value of the dipole projected along the H-bonded nitrogen atoms.

Table S3: Absolute molecular dipoles values projected along the H-bonded N atoms obtained from the energy minimum, thermal classical (MD) and quantum (PIMD) average. Dipoles are expressed in Debye.

	trans	*cis*	MD	PIMD
Dipole	0.0	1.2	0.3	0.5

Additional Information on Free Energy Profiles

In Fig. S1 we show the effective free energy profile for the hydrogen transfer coordinate obtained from PIMD simulations at 290K using PBE+MBD as exchange correlation functional. These are qualitatively different from the rest of the simulations where the B3LYP+TS functional was used. In this case, the combination of the small proton transfer barrier height and ZPE produce a total delocalization of the protons.

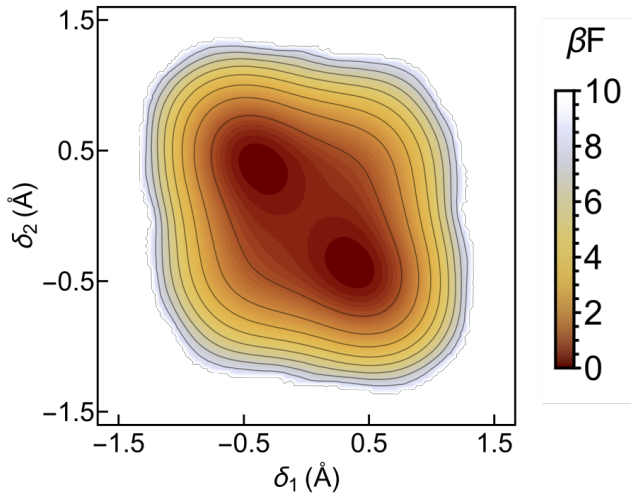

Figure S1: Effective free energy profile for the hydrogen transfer coordinate obtained from PIMD simulations at 290K using PBE+MBD exchange correlation functional. The contour lines are separated by 1 k_BT.

In Fig. S2 and S3 we show the same free energy profile at 100K with B3LYP+TS exchange correlation functional and in Fig. S4 we present the 1D free energy cuts along the *trans-trans*, *cis-cis* and *trans-cis* paths. Finally in Fig. S5 we show the regions considered to compute the *trans/cis* population ratio.

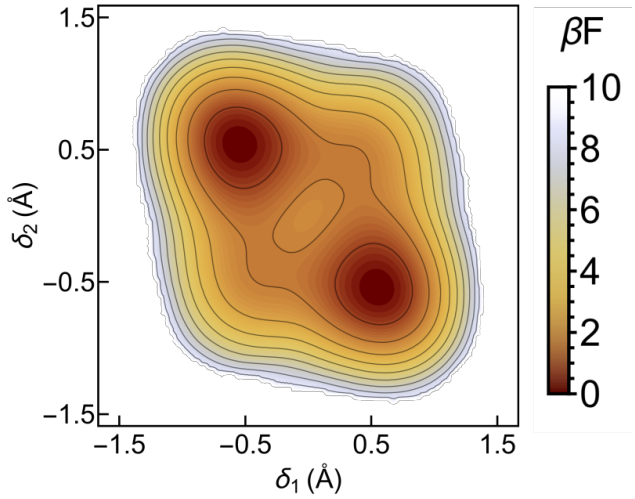

Figure S2: Effective free energy profile for the hydrogen transfer coordinate obtained from PIMD simulations at 100K. The contour lines are separated by 1 k_BT starting at 0.75 k_BT.

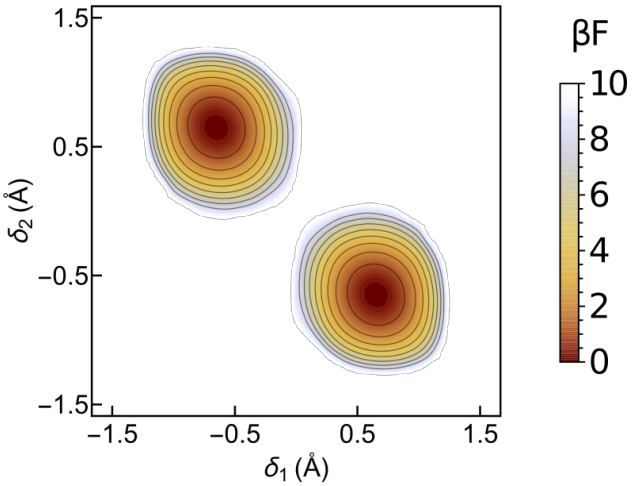

Figure S3: Effective free energy profile for the hydrogen transfer coordinate obtained from MD simulations at 290K. The contour lines are separated by 1 k_bT.

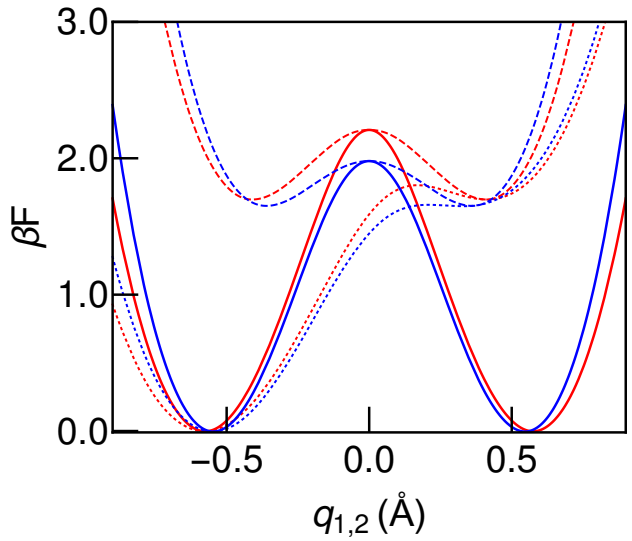

Figure S4: Effective free energy projections along q_1, $\delta_1 = -\delta_2$, (solid lines), q_2, $\delta_1 = \delta_2$, (dashed lines) and q_3, path connecting trans and cis, (dotted lines) directions. Red and blue lines correspond to PIMD simulations at 290K and 100K respectively.

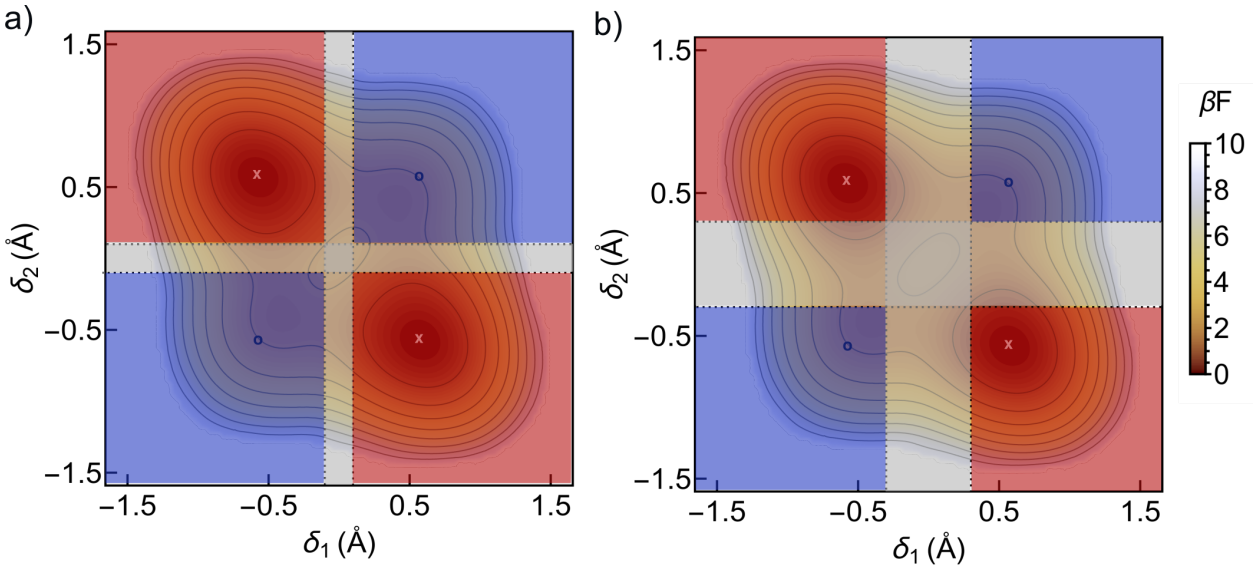

Figure S5: Effective free energy profile of the porphycene molecule obtained from PIMD simulations at 290K, projected on the δ_1 and δ_2 coordinates. Red and blue regions show the population that is considered as *trans* ($\{\delta_1 > b \cap \delta_2 < -b\} \cup \{\delta_1 < -b \cap \delta_2 > b\}$ and *cis* ($\{\delta_1 > b \cap \delta_2 > b\} \cup \{\delta_1 < -b \cap \delta_2 < -b\}$) respectively with boundaries $b = 0.1$ (a) and $b = 0.3$ (b). Structures that fall in the gray area are considered transition-state-like structures and therefore discarded.

Additional Information on Instanton Calculations

The ring-polymer instanton calculations were performed using the standard procedure described elsewhere.[17,18] In this theory, the thermal rate is given by the expression[19]

$$k_{\text{inst}} Q_{\text{reac}} = \frac{1}{\beta_P \hbar} \sqrt{\frac{B_N}{2\pi \beta_P \hbar^2}} Q_{\text{inst}} e^{-S/\hbar}, \tag{1}$$

where Q_{reac} and Q_{inst} refers to the reactant and instanton partition functions respectively, S is the instanton action obtained as $\beta_P \hbar U_P(\tilde{q})$ where U_P is the potential energy (including the spring term) of the extended ring-polymer Hamiltonian and $\tilde{q}$ is the geometry of the instanton. B_N is a normalization factor, $\beta_P = \beta/P$ with $\beta = 1/k_B T$ and P is the number of replicas of the system used. A more detailed definition of these factors can be found in Ref.[18] In table S4 we show the convergence of the rates at 100 and 150 K with respect to

the number of beads.

Table S4: Convergence with number of replicas of the ring-polymer instanton thermal rate obtained with B3LYP+TS functional at 100K and 150K. Rates are expressed in units of $(10^{11}s^{-1})$

Number of replicas	Rate at 100K	Rate at 150K
64	0.3	1.2
192	0.6	2.1
256	0.6	2.2

The correction factor that was used to scale the B3LYP+TS barrier to the CCSD(T) ones can be read as following:

$$\begin{aligned} S^{corrected} &= \beta_P \hbar U_P^{corrected}(\tilde{q}) \\ &= \beta_P \hbar \sum_k^P \sum_i^{3N} \left[\frac{m_i}{2(\beta_P \hbar)^2} (\tilde{q}_i^{(k)} - \tilde{q}_i^{(k+1)})^2 \right] + f \sum_k^P V^{(k)}(\tilde{q}_1^{(k)}, \ldots, \tilde{q}_{3N}^{(k)}), \end{aligned} \tag{2}$$

where $\tilde{q}_i^{(k)}$ represents the position of the i-th degree of freedom at the imaginary time slice k evaluated at the instanton geometry, N is the number of atoms, which is 38 for the porphycene molecule, and f is the correction factor defined as the ratio of the energy barriers obtained with CCSD(T) and B3LYP+TS for the considered path. It is assumed that the zero of energy is set the reactant.

In Fig. S6 we show the potential energy along the cumulative mass-weighted path-length and in Fig. S7 we present the 2D projection of the instanton pathways in the δ_1 and δ_2 plane.

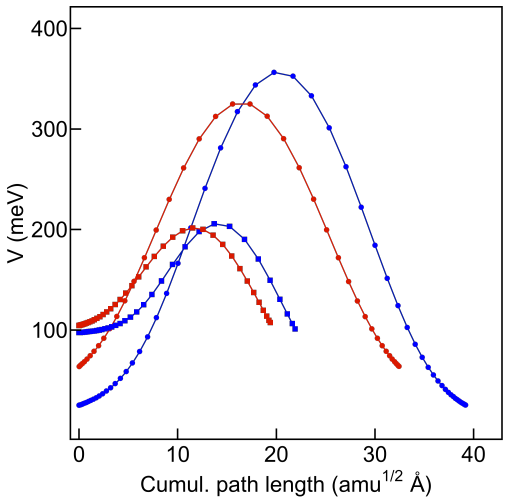

Figure S6: Potential energy along the cumulative mass-weighted path-length[20] at 150 K (red) and 100K (blue) for concerted (circles) and stepwise (squares) mechanisms. The zero of energy is set at the trans minimum energy geometry. This is the actual barrier which the system must tunnel through and clearly shows that the concerted path-length is longer.

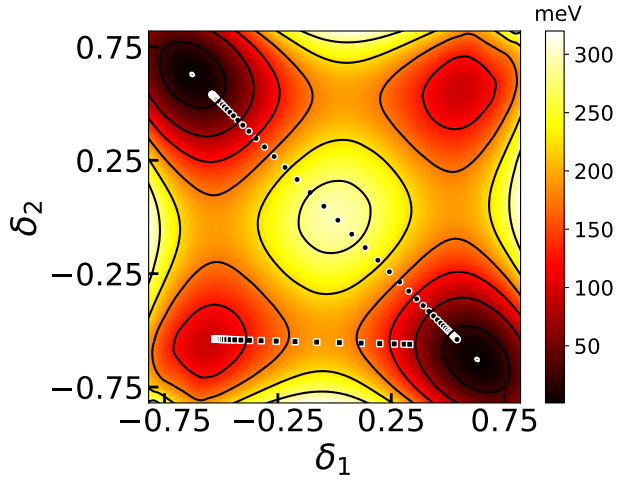

Figure S7: 2D projection of the instanton geometry in the δ_1 and δ_2 plane at 100K. Each circle and square represents one replica of the discretized concerted and stepwise tunnelling pathway respectively. White dots are placed at the corresponding *trans* and *cis* minimum-energy geometry for reference.

Derivation of the Ring-Polymer Expansion of the Hessian used in the Instanton Calculations

In this section, we demonstrate the the ring-polymer expansion of the Hessian. We make use of the transformation matrix $T(P, P')$ defined in the Ref.,[21] where P and P' are the old (smaller) and new (larger) number of beads, defining the contraction operation as

$$r_i^{(k)} = \sum_j^{P'} (T(P, P'))_{kj} R_i^{(j)}, \tag{3}$$

where $r_i^{(k)}$ is the i position component corresponding to the *k-th* old replica and $R_i^{(j)}$ is the i position component corresponding to the *j-th* new replica.

The $P' \times P$ expansion matrix $T(P', P)$ can be defined as

$$(T(P', P))_{kj} = \frac{P'}{P} (T(P, P'))_{kj}^t. \tag{4}$$

It can be shown that this matrix has the following properties:

$$\sum_j (T(P', P))_{ij} = 1 \tag{5}$$

$$\sum_i (T(P', P))_{ij} = \frac{P'}{P}. \tag{6}$$

We start our derivation with the following approximation

$$\mathcal{V}^{(k)} \approx \sum_j^P T(P', P))_{kj} V^{(j)}, \tag{7}$$

where $\mathcal{V}^{(k)}$ represents the potential energy corresponding to the *k-th* new replica and $V^{(j)}$ represents the potential energy corresponding to the *k-th* old replica. Summing over k and

using the properties of the T matrix we get the well known expression

$$\sum_{k}^{P'} \mathcal{V}^{(k)} \approx \sum_{j}^{P} \frac{P'}{P} V^{(j)}. \tag{8}$$

Applying the chain rule , the forces can be approximated as

$$\begin{aligned}
\mathcal{F}_j^{(k)} &= -\frac{\partial\Big[\sum_l^{P'} \mathcal{V}^{(l)}\Big]}{\partial R_j^{(k)}} \\
&\approx -\frac{\partial\Big[\frac{P'}{P}\sum_l^{P} V^{(l)}\Big]}{\partial R_j^{(k)}} = -\sum_m^P \frac{\partial\Big[\frac{P'}{P}\sum_l^{P} V^{(l)}\Big]}{\partial r_j^{(m)}} \times \frac{\partial r_j^{(m)}}{\partial R_j^{(k)}} = -\sum_m^P \frac{\partial\Big[\frac{P'}{P}\sum_l^{P} V^{(l)}\Big]}{\partial r_j^{(m)}} (T(P,P'))_{mk} \\
&= \frac{P'}{P}\sum_m^P\sum_l^P \frac{-\partial V^{(l)}}{\partial r_j^{(m)}} (T(P,P'))_{mk} = \frac{P'}{P}\sum_l^P \frac{-\partial V^{(l)}}{\partial r_j^{(l)}} (T(P,P'))_{lk} = \frac{P'}{P}\sum_l^P F_j^{(l)} (T(P,P'))_{lk} \\
&= \sum_l^P F_j^{(l)} (T(P',P))_{kl}.
\end{aligned} \tag{9}$$

where $\mathcal{F}_j^{(k)}$ is the j force component corresponding to the *k-th* new replica, $F_f^{(l)}$ is the j force component corresponding to the *l-th* old replica and the fact that $\frac{-\partial V^{(l)}}{\partial r_j^{(m)}} = \delta_{lm}$ was used. Since the force comes from the derivative of Eq. 7, one needs to sum again over k and use the properties of the T matrix to get

$$\sum_{k}^{P'} \mathcal{F}_j^{(k)} \approx \sum_{j}^{P} \frac{P'}{P} F_j^{(l)}. \tag{10}$$

Applying the chain rule a second time to Eq. 10, one can obtain the expression for the

ring polymer expansion of the Hessian following similar steps.

$$\begin{aligned}\mathcal{H}_{jm}^{(k)} &= -\frac{\partial\Big[\sum_l^{P'} \mathcal{F}_j^{(l)}\Big]}{\partial R_m^{(k)}} \\ &\approx -\frac{\partial\Big[\frac{P'}{P}\sum_l^{P} f_j^{(l)}\Big]}{\partial R_m^{(k)}} = -\sum_s^P \frac{\partial\Big[\frac{P'}{P}\sum_l^{P} f_j^{(l)}\Big]}{\partial r_m^{(s)}} \times \frac{\partial r_m^{(s)}}{\partial R_m^{(k)}} = -\sum_s^P \frac{\partial\Big[\frac{P'}{P}\sum_l^{P} f_j^{(l)}\Big]}{\partial r_m^{(s)}} (T(P,P'))_{sk} \\ &= \frac{P'}{P}\sum_s^P \frac{-\partial f_j^{(s)}}{\partial r_m^{(s)}} (T(P,P'))_{sk} = \sum_s^P H_{jm}^{(s)} (T(P',P))_{ks},\end{aligned} \tag{11}$$

where $H_{jm}^{(s)}$ is the jm matrix element of the Hessian corresponding to the *s-th* old replica and $\mathcal{H}_{jm}^{(k)}$ is the jm matrix element of the Hessian corresponding to the *k-th* new replica.

Additional Information on IR Spectra

In Fig. S8 we present the vibrational density of states (290 K) of a water molecule calculated with thermostatted ring polymer molecular dynamics (TRPMD) coupled to colored noise thermostats on the Partridge-Schwenke potential.[22] We show that convergence is reached at 16 beads in this case. We thus simulated the IR spectrum of porphycene at 290 K with 16 beads in this paper.

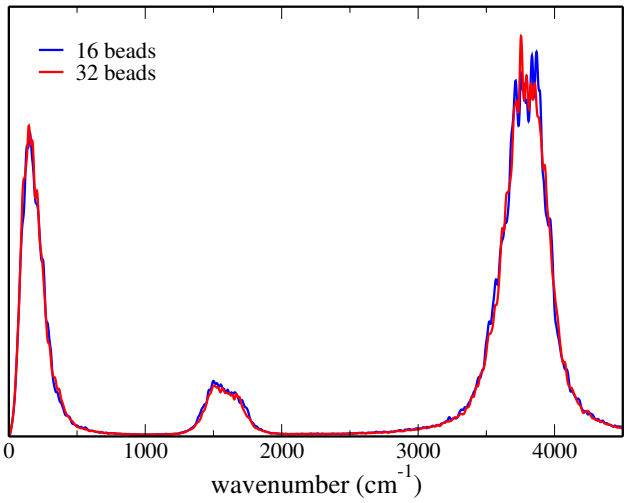

Figure S8: Vibrational density of states of a water molecule from TRPMD employing 16 and 32 beads. Each one was computed by two independent 85 ps trajectories.

In Fig S9 we show the IR spectra obtained with the PBE+MBD functional. In the harmonic spectrum (a), the N-H stretching band presents a red shift of 350 cm^{-1} with respect to the one obtained with B3LYP+TS, which is not surprising since GGA xc functionals are known to overestimate the hydrogen bond strength. The inclusion of anharmonicity and temperature effects in the molecular dynamics spectrum (b) produces a similar effect to what is observed in the B3LYP+TS simulation, i.e a broadening and a slight red shift of the N-H band with respect to the corresponding harmonic case. The subsequent inclusion of nuclear quantum effects from thermostatted ring polymer molecular dynamics shows an absence of the N-H band in that region of the spectrum presented in (c), which is completely different from B3LYP+TS simulation. This difference is easy to rationalize. The PBE+MBD functional predicts a low barrier which is smaller than the ZPE correction (negative values in the second column of Table S1) and therefore, the hydrogen transfer barrier disappears. As already mentioned, this fact gives rise to a total delocalization of the hydrogen atoms which can be observed not only in the free energy profile but also in the IR spectrum. In panel (d), where the hydrogen atoms in the cage are substituted by deuterium, the barrier is still present after ZPE corrections, since these are smaller for deuterium. Therefore, a localized broad peak is observed at the mass scaled frequency ($\approx$ 1700 cm^{-1}). Finally, it is worth noting that the apparent agreement of the classical-nuclei simulation with the experimental one for this xc functional is completely fortuitous and for the wrong physical reasons. Hence, the presented results in the main manuscript are based on simulations performed with B3LYP+TS xc functional which captures the right physics.

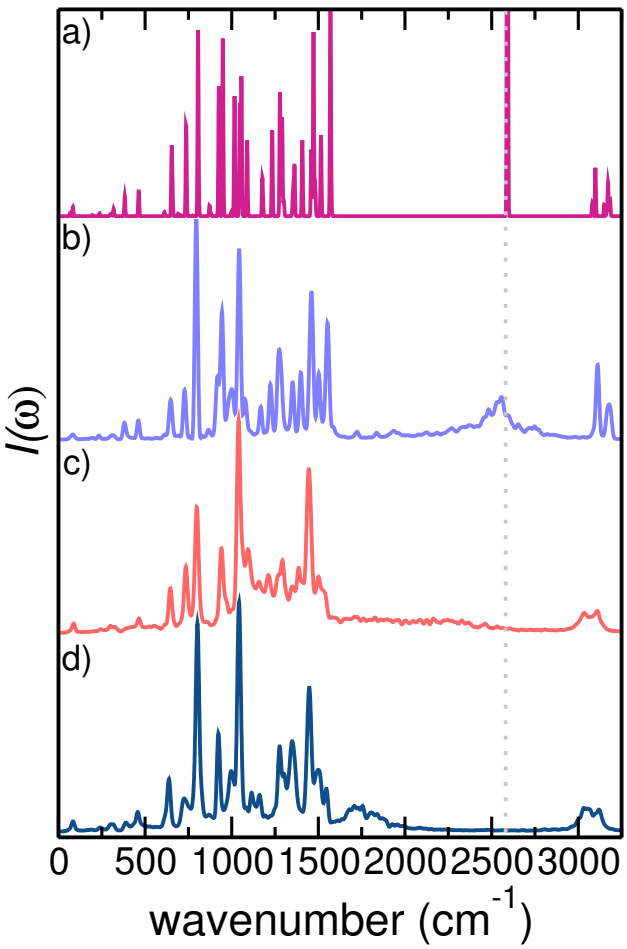

Figure S9: IR spectra obtained with the PBE+MBD functional including many body dispersion interactions.[12] a) Harmonic approximation, b) Fourier transform of dipole autocorrelation function from (classical-nuclei) molecular dynamics, c) Fourier transform of dipole autocorrelation function from thermostatted ring polymer molecular dynamics (quantum nuclei), d) Fourier transform of dipole autocorrelation function from thermostatted ring polymer molecular dynamics (quantum nuclei) with the hydrogen atoms in the cage substituted by deuterium (DD).

Model of coupled quantum harmonic oscillators

We used the methodology developed by Henri-Rousseau and Blaise.[23] The full Hamiltonian in the absence of damping may be written as

$$H_{\text{tot}} = H_{\text{fast}} + H_{\text{slow}}. \tag{12}$$

H_{fast} and H_{slow} are given by

$$H_{\text{fast}} = \frac{p^2}{2m} + \frac{1}{2}m\omega(Q)q^2, \tag{13}$$

and

$$H_{\text{slow}} = \frac{P^2}{2M} + \frac{1}{2}M\Omega Q^2, \tag{14}$$

where q, Q, p, P, m ,M, ω and Ω correspond to the position, conjugate momenta, mass and frequency of the fast and slow mode respectively. The angular frequency of the fast mode is expanded up to first order obtaining

$$\omega(Q) = \omega^{\circ} + bQ, \tag{15}$$

where ω° is the fast mode frequency in absence of coupling. One may define a convenient dimensionless coupling parameter α as

$$\alpha = \frac{b}{\Omega}\sqrt{\frac{\hbar}{2M\Omega}}. \tag{16}$$

Consequently, using the adiabatic approximation to decouple the fast and slow degrees of motion and with the introduction of direct (γ) and indirect (γ°) damping, one arrives to the following expression of the spectral density (SD):

$$SD(t) \propto e^{i\omega^{\circ}t}(e^{i2\alpha^2\Omega t})(e^{i2\alpha^2 e^{-\gamma t/2}sin(\Omega t)})\left[(e^{\alpha^2[\langle n\rangle+\frac{1}{2}](2e^{-\gamma t/2}cos(\Omega t)-e^{-\gamma t}-1)}\right](e^{-\gamma^{\circ}t}), \tag{17}$$

where $\langle n\rangle = 1/(e^{\hbar\Omega/k_BT})$, k_B is the Boltzmann constant and T is the absolute temperature. Finally the SD in the frequency space is obtained by the Fourier transform of Eq. 18. In table S5 we show the range of parameters used to reproduce the simulated TRPMD spectrum of porphycene. In Fig. S10 two illustrative examples of the spectra obtained with those parameters are presented.

Table S5: Range of parameters that yield a good agreement for the TRPMD spectrum of porphycene.

Ω (cm^{-1})	ω° (cm^{-1})	α	γ (Ω)	γ° (Ω)
100-115	2680-2750	0.70-0.85	0.1-0.2	0.2-0.3

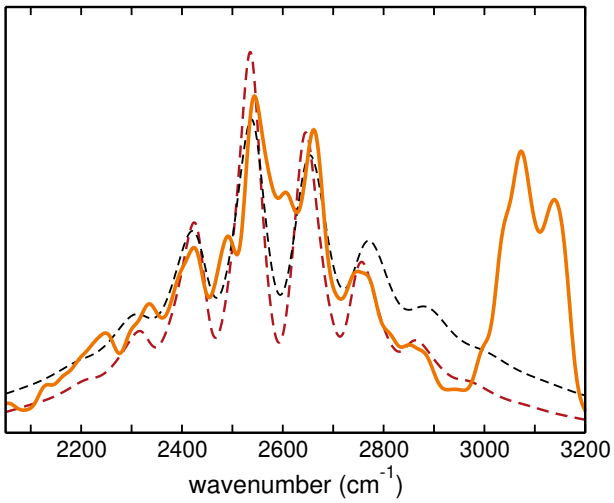

Figure S10: Fourier transform of the dipole autocorrelation function obtained with TRPMD in the N-H stretching band region (orange), adiabatic model with Ω= 110 cm^{-1}, ω° = 2740 cm^{-1} , α = 0.85 , γ = 0.3 Ω, γ° = 0.2 Ω(dashed red) and adiabatic model with Ω= 105 cm^{-1}, ω° = 2680 cm^{-1} , α = 0.70 , γ = 0.23 Ω, γ° = 0.1 Ω (dashed red).

We could also compute b values by finite difference displacements of the harmonic normal modes of porphycene (Eq. 13) and convert them to the corresponding α using the Eq. 16. In table we report the computed α coupling parameter of all modes with both symmetric and antymmetric N-H stretch. We used the following definition of M_i (the generalized mass of the i-th mode) needed to convert b into α

$$\frac{1}{M_i} = \sum_i \frac{|a_i^j|^j}{m_j}, \tag{18}$$

where m_j is the mass of the j-th degree of freedom, and $|a_i^j|^j$ is the j-th element of the i-th normalized normal mode eigenvector. The values for α are shown in the table below.

Ω (cm^{-1})	$\alpha_1 \times 10^3$	$\alpha_2 \times 10^3$
66	0.4	0.7
74	-0.3	0.8
87	0.3	-0.3
121	-0.5	0.6
133	0.3	0.6
153	2.8	3.9
197	-17.5	-17.8
199	-0.6	-0.4
202	-0.1	1.3
207	0.4	0.2
245	0.7	-2.1
313	0.0	0.8
320	-0.5	0.9
329	-0.6	-1.3
352	1.7	2.4
374	-1.2	-2.2
395	-0.1	-0.2
403	-0.3	-0.4
475	0.3	-0.6
495	2.3	1.5
495	2.0	1.3
517	0.3	-0.3
613	-2.7	-1.6
629	0.0	0.7
641	-0.1	0.2
646	0.0	0.0

Ω (cm^{-1})	$\alpha_1 \times 10^3$	$\alpha_2 \times 10^3$
672	-0.1	-0.2
673	-0.0	-0.0
678	2.5	2.2
679	-0.1	0.3
711	0.1	-0.1
713	0.1	0.1
718	-0.0	0.2
728	0.2	-0.2
763	0.0	0.1
779	-0.0	-0.1
789	0.2	-0.0
799	-0.0	0.1
832	0.6	0.6
833	0.3	0.1
835	-4.1	-4.1
839	-0.1	-0.3
883	-2.6	-2.2
902	0.0	-0.3
907	0.0	-0.2
910	-0.1	0.1
912	0.1	-0.0
914	0.0	0.0
942	-0.2	-0.1
949	0.2	-0.1
960	-0.0	0.2
964	0.1	-0.1

Ω (cm^{-1})	$\alpha_1 \times 10^3$	$\alpha_2 \times 10^3$
965	-0.0	0.1
988	0.0	-0.2
992	-0.0	0.3
994	-3.3	-3.2
1012	-2.1	-2.2
1026	-0.1	-0.0
1070	0.1	0.1
1080	-2.9	-3.9
1086	0.1	-0.1
1091	-1.6	-1.2
1119	0.1	0.0
1138	-1.7	-1.8
1185	1.2	1.8
1199	-0.1	0.2
1221	-0.1	0.2
1238	0.8	1.3
1259	-0.0	-0.0
1274	-0.0	0.2
1283	2.5	2.3
1300	3.6	3.8
1315	0.1	-0.2
1326	0.2	-0.0
1356	-0.5	-0.3
1374	1.8	1.6
1389	-0.1	0.2
1396	0.5	0.1

Ω (cm^{-1})	$\alpha_1 \times 10^3$	$\alpha_2 \times 10^3$
1405	0.0	0.1
1430	-0.8	-0.1
1436	-1.4	-1.8
1446	0.1	0.0
1475	-3.3	-3.6
1492	-0.0	-0.0
1499	0.0	0.0
1520	0.1	0.0
1521	2.9	3.3
1547	3.2	3.3
1554	-0.1	0.0
1574	0.6	0.2
1593	0.8	0.5
1602	-0.0	0.0
1618	-0.0	0.0
1650	3.8	3.7
2902	25.4	25.3
2905	0.1	-0.1
3167	-0.1	0.1
3167	0.0	-0.0
3186	0.0	0.2
3187	0.0	-0.0
3238	0.1	0.0

Ω (cm^{-1})	$\alpha_1 \times 10^3$	$\alpha_2 \times 10^3$
3238	-0.0	-0.0
3252	0.0	0.2
3253	-0.0	0.0
3258	-0.0	-0.3
3260	-0.0	0.0
3270	-0.1	-0.2
3273	-0.0	0.0

Table S6: Dimensionless coupling parameter between harmonic modes with symmetric (α_1, $\omega = 2902cm^{-1}$) and antisymmetric (α_2,$\omega = 2905cm^{-1}$) N-H stretching motion.

References

(1) Riplinger, C.; Sandhoefer, B.; Hansen, A.; Neese, F. Natural triple excitations in local coupled cluster calculations with pair natural orbitals. *J. Chem. Phys.* **2013**, *139*, 134101.

(2) Møller, C.; Plesset, M. S. Note on an Approximation Treatment for Many-Electron Systems. *Phys. Rev.* **1934**, *46*, 618–622.

(3) Neese, F. The ORCA program system. *Wiley Interdiscip. Rev.: Comp. Mol. Sci.* **2012**, *110*, 73–78.

(4) Dunning, T. H. Gaussian basis sets for use in correlated molecular calculations. I. The atoms boron through neon and hydrogen. *J. Chem. Phys.* **1989**, *90*, 1007–1023.

(5) Karton, A.; Martin, J. M. L. Comment on: "Estimating the Hartree-Fock limit from finite basis set calculations" [Jensen F (2005) Theor Chem Acc 113:267]. *Theor. Chem. Acc.* **2006**, *115*, 330–333.

(6) Truhlar, D. G. Basis-set extrapolation. *Chem. Phys. Lett.* **1998**, *294*, 45–48.

(7) Perdew, J. P.; Burke, K.; Ernzerhof, M. Generalized Gradient Approximation Made Simple. *Phys. Rev. Lett.* **1996**, *77*, 3865–3868.

(8) Adamo, C.; Barone, V. Toward reliable density functional methods without adjustable parameters: The PBE0 model. *J. Chem. Phys.* **1999**, *110*, 6158–6170.

(9) Becke, A. D. DensityâĂŘfunctional thermochemistry. III. The role of exact exchange. *J. Chem. Phys.* **1993**, *98*, 5648–5652.

(10) Stephens, P. J.; Devlin, F. J.; Chabalowski, C. F.; Frisch, M. J. Ab Initio Calculation of Vibrational Absorption and Circular Dichroism Spectra Using Density Functional Force Fields. *J. Phys. Chem.* **1994**, *98*, 11623–11627.

(11) Tkatchenko, A.; Scheffler, M. Accurate Molecular Van Der Waals Interactions from Ground-State Electron Density and Free-Atom Reference Data. *Phys. Rev. Lett.* **2009**, *102*, 073005.

(12) DiStasio Jr, R. A.; Gobre, V. V.; Tkatchenko, A. Many-body van der Waals interactions in molecules and condensed matter. *J. Phys. Cond. Matt.* **2014**, *26*, 213202.

(13) Blum, V.; Gehrke, R.; Hanke, F.; Havu, P.; Havu, V.; Ren, X.; Reuter, K.; Scheffler, M. Ab initio molecular simulations with numeric atom-centered orbitals. *Comp. Phys. Comm.* **2009**, *180*, 2175 – 2196.

(14) Kozlowski, P. M.; Zgierski, M. Z.; Baker, J. The inner-hydrogen migration and ground-state structure of porphycene. *J. Chem. Phys.* **1998**, *109*, 5905–5913.

(15) Smedarchina, Z.; Siebrand, W.; Fernández-Ramos, A. Tunneling splitting in double-proton transfer: Direct diagonalization results for porphycene. *J. Chem. Phys.* **2014**, *141*, 174312.

(16) Vogel, E.; Köcher, M.; Schmickler, H.; Lex, J. Porphycene - a Novel Porphin Isomer. *Angew. Chem. Int. Ed.* **1986**, *25*, 257–259.

(17) Kapil, V.; Rossi, M.; Marsalek, O.; Petraglia, R.; Litman, Y.; Spura, T.; Cheng, B.; Cuzzocrea, A.; Meißner, R. H.; Wilkins, D. M.; Juda, P.; Bienvenue, S. P.; Fang, W.; Kessler, J.; Poltavsky, I.; Vandenbrande, S.; Wieme, J.; Corminboeuf, C.; Kühne, T. D.; Manolopoulos, D. E.; Markland, T. E.; Richardson, J. O.; Tkatchenko, A.; Tribello, G. A.; Speybroeck, V. V.; Ceriotti, M. i-PI 2.0: A universal force engine for advanced molecular simulations. *J. Chem. Phys.* **2018**, In Press, DOI:10.1016/j.cpc.2018.09.020.

(18) Richardson, J. O. Ring-polymer instanton theory. *Int. Rev. Phys. Chem.* **2018**, *37*, 171–216.

(19) Richardson, J. O.; Althorpe, S. C. Ring-polymer molecular dynamics rate-theory in the deep-tunneling regime: Connection with semiclassical instanton theory. *J. Chem. Phys.* **2009**, *131*, 214106.

(20) Beyer, A. N.; Richardson, J. O.; Knowles, P. J.; Rommel, J.; Althorpe, S. C. Quantum Tunneling Rates of Gas-Phase Reactions from On-the-Fly Instanton Calculations. *J. Phys. Chem. Lett.* **2016**, *7*, 4374–4379.

(21) Markland, T. E.; Manolopoulos, D. E. An efficient ring polymer contraction scheme for imaginary time path integral simulations. *J. Chem. Phys.* **2008**, *129*, 024105.

(22) Partridge, H.; Schwenke, D. W. The determination of an accurate isotope dependent potential energy surface for water from extensive ab initio calculations and experimental data. *J. Chem. Phys.* **1997**, *106*, 4618–4639.

(23) Henri-Rousseau, O.; Blaise, P. *Adv. Chem. Phys.*; Wiley-Blackwell, 2008; Chapter 5, pp 245–496.